

Multiscale Hodge Scattering Networks for Data Analysis

Naoki Saito*, Stefan C. Schonsheck, Eugene Shvarts

^a*Department of Mathematics, University of California, Davis, One Shields Avenue, Davis, 95616, CA, USA*

Abstract

We propose new scattering networks for signals measured on simplicial complexes, which we call *Multiscale Hodge Scattering Networks* (MHSNs). Our construction is based on multiscale basis dictionaries on simplicial complexes, i.e., the κ -GHWT and κ -HGLET, which we recently developed for simplices of dimension $\kappa \in \mathbb{N}$ in a given simplicial complex by generalizing the node-based Generalized Haar-Walsh Transform (GHWT) and Hierarchical Graph Laplacian Eigen Transform (HGLET). The κ -GHWT and the κ -HGLET both form redundant sets (i.e., dictionaries) of multiscale basis vectors and the corresponding expansion coefficients of a given signal. Our MHSNs use a layered structure analogous to a convolutional neural network (CNN) to cascade the moments of the modulus of the dictionary coefficients. The resulting features are invariant to reordering of the simplices (i.e., node permutation of the underlying graphs). Importantly, the use of multiscale basis dictionaries in our MHSNs admits a natural pooling operation that is akin to local pooling in CNNs, and which may be performed either locally or per-scale. These pooling operations are harder to define in both traditional scattering networks based on Morlet wavelets, and geometric scattering networks based on Diffusion Wavelets. As a result, we are able to extract a rich set of descriptive yet robust features that can be used along with very simple machine learning methods (i.e., logistic regression or support vector machines) to achieve high-accuracy classification systems with far fewer number of parameters to train than most modern graph neural networks. Finally, we demonstrate the usefulness of our MHSNs in three distinct types of problems: signal classification, domain (i.e., graph/simplex) classification, and molecular dynamics prediction.

Keywords: Scattering transform, simplicial complexes, multiscale graph basis dictionaries, Hodge Laplacians, Haar-Walsh wavelet packets, graph classification, signal classification and regression

1. Introduction

Scattering Transforms were introduced by Mallat in [1] as a method for feature extraction for signals and images. These features are translation quasi-invariant, stable to deformation, and preserve high-frequency information from the input which make them ideal for a wide variety of data classification problems, e.g., texture image classification

*Corresponding author

Email addresses: saito@math.ucdavis.edu (Naoki Saito), sschonsh@gmail.com (Stefan C. Schonsheck), eugene.shvarts@gmail.com (Eugene Shvarts)

[2, 3]. In addition, their computational architecture closely resembles a convolutional neural networks (CNNs), which allows for fast, GPU-friendly computation. In fact, these networks are often thought of as a type of CNN, with predetermined wavelet filter banks as their convolution filters and a pointwise modulus operation as their activation function. A key advantage of these networks over traditional CNNs is that since the filter banks do not need to be learned from input data, they are much less data-hungry. Additionally, they are more interpretable since each channel in the hidden representation is a deterministic cascade of wavelet transform convolutions with nonlinear activation and averaging operators.

More recently, Gao et al. introduced an analogous network architecture for node-signals on undirected graphs [4], which they named as “Geometric Scattering (Networks).” In this context, invariance to node-permutation takes the place of translation-invariance. This is achieved in a manner similar to PointNet [5], by aggregating the node features through either a sum or max-values operation into a single value for each channel. This leads to a deformation-stable feature extractor that can be utilized in concert with a very simple learning model (normally logistic regression or support vector machine) to achieve near state-of-the-art classification results on many datasets, with far fewer training examples than CNN-based approaches often require. As a result, these networks generate descriptive yet robust features that can be used along with very simple machine learning methods (i.e., support vector machines or logistic regression) to achieve high-accuracy classification systems with only small amounts of training data and with far fewer number of parameters to train.

In this article, we advance this line of research to apply to signals defined on arbitrarily high-dimensional simplicial structures, i.e., edges, triangles, pyramids, and their κ -dimensional analogs. Our methods differ from previous work in two key ways. First, previous scattering transform networks have applied only to point-valued signals whereas our construction generalizes to high-dimensional structures. Second, we utilize the κ -Hierarchical Graph Laplace Transforms (κ -HGLET) [6, 7] and κ -Generalized Haar-Walsh Transform (κ -GHWT)[8, 7] as the wavelet banks in the transforms. Previous work has mostly been based on Morlet wavelets for images and Diffusion Wavelets [9] for graph-based signals. However, we find that the bipartition tree induced by the multiscale transforms we proposed in [7] allows us to form sparser approximations which in turn lead to more efficient feature extraction and therefore more expressive networks. Additionally, the multiscale structure of these bases allows us to easily define local pooling operations which can boost the performance of scattering networks in many applications.

1.1. Comparison with Related Works

There has been a growth in recent interest in studying signals defined on edges, triangles, and higher-dimensional substructures within graph structured data [10, 11, 12, 13, 14]. Applications in computer vision [15, 16], statistics [17], topological data analysis [14, 18], and network analysis [19] have benefited from the study of high-dimensional simplicial complexes. Convolution-based simplicial neural networks have shown remarkable results in these new domains [20]. We extend this line of research by defining scattering networks on these higher-dimensional domains.

Scattering networks [2] were initially introduced as a tool to explain the success of CNNs on many computer vision problems. These networks had many of the invariant

and equivariant properties that make CNNs desirable, but did not contain any learnable ‘filters’, and instead employed a cascade of wavelet convolutions and contractive nonlinearities. Later, Gao et al. successfully generalized these networks to apply to graph convolutional networks [4]. Our work further generalizes these approaches.

The main ways our MHSNs differ from Geometric Scattering Networks (GSNs) [4] and Deep Haar Scattering Networks (DHSNs) [21] are: 1) MHSNs accept arbitrary simplicial complexes while GSNs/DHSNs were designed for nodes only; and 2) GSNs and DHSNs are based on the Diffusion Wavelets of Coifman and Maggioni [9] and the Haar transform, respectively, and hence they are not based on the hierarchical partitioning of a given graph, while MHSNs are built over the richer HGLET/GHWT dictionaries and more amenable for analysis since they are composed of a collection of orthonormal bases (ONBs). Hodgelets [22] use a kernel defined in the spectral domain, similar to the spectral graph wavelet transform [23] to define another family of wavelet-like frames for signals on simplicial complexes. Topological Slepians [24] also form a localized basis dictionary on a given collection of κ -simplices, but their construction is based on the maximization of primal domain concentration of vectors subject to the dual domain (the frequency domain) support set. However, both Hodgelets and Topological Slepians are difficult to use for scattering transform type representations since they are not hierarchically arranged.

Recently, Chew et al. introduced a method for *windowed* scattering transforms which achieve local-pooling like operations [25]. However, since the underlying topology of the graph/complex is non-Euclidean, it may be difficult to consistently define the local windows across multiple graphs [26, 27]. It may be possible to use the partitioning scheme proposed in [7] for these windows, but defining appropriate wavelet families for such a hybrid approach requires further study.

2. Hodge Laplacians and Multiscale Basis Dictionaries

In this section we review some basic Hodge theory to define the Hodge Laplacian on simplicial complexes and then summarize the construction of multiscale basis functions on these spaces. For a more thorough introduction into Hodge Theory see [10, 12, 16] and for a more detailed explanation of multiscale basis dictionaries see [28, 7].

2.1. Simplicial Complexes and Boundary Operators

In this subsection we review concepts from algebraic topology to formally define simplicial complexes and introduce some notions of how two simplices can be “adjacent.” For a more thorough review, see [10, 12]. Given a vertex (or node) set $V = \{v_1, \dots, v_n\}$, a κ -*simplex* σ is a $(\kappa + 1)$ -subset of V . A *face* of σ is a κ -subset of σ , and so σ has $\kappa + 1$ faces. A *co-face* of σ is a $(\kappa + 1)$ -simplex, of which σ is a face. A *simplicial complex* C is a collection of simplices closed under subsets, where if $\sigma \in C$, then $\alpha \subset \sigma \implies \alpha \in C$. In particular, if $\sigma \in C$, so does each face of σ . Let $\kappa_{\max}(C) := \max\{\kappa \mid \sigma \in C \text{ is a } \kappa\text{-simplex}\}$, and for each $\kappa \in \{0, 1, \dots, \kappa_{\max}\}$, let C_κ denote the set of κ -simplices in C , and let X_κ be the space of real-valued functions on C_κ . When $\kappa > \kappa_{\max}$, $C_\kappa = \emptyset$. We also refer to C as a κ -*complex* to note that $\kappa_{\max}(C) = \kappa$. Let a κ -*region* of C refer to any nonempty subset of C_κ .

Let C be a simplicial complex, and $\sigma, \tau \in C_\kappa$, for some $\kappa > 0$. When σ, τ share a face, they are *weakly adjacent*, denoted by $\sigma \sim \tau$. When $\sigma \sim \tau$, additionally they both

share a co-face, their *hull*, denoted by $\text{hl}(\sigma, \tau)$. If $\sigma, \tau \in C$, $\sigma \sim \tau$, and $\text{hl}(\sigma, \tau) \in C$, then σ, τ are *strongly adjacent*, denoted by $\sigma \simeq \tau$. If $\sigma \sim \tau$, but $\sigma \not\sim \tau$ in C , then σ, τ are κ -*adjacent*, denoted $\sigma \underset{\kappa}{\sim} \tau$. Figure 1 demonstrates these various adjacencies among simplices in a toy 2-complex.

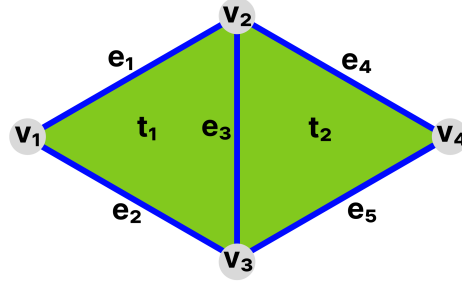


Figure 1: In this small 2-complex C , $e_1 \sim e_4$ because they share the face v_2 , and $e_1 \sim e_2$ because they share the face v_1 . Further $e_1 \simeq e_2$ because their hull $t_1 \in C$, but $e_1 \not\sim e_4$, so that $e_1 \underset{1}{\sim} e_4$. We have $t_1 \sim t_2$ because they share the face e_3 , and also $t_1 \underset{2}{\sim} t_2$.

Suppose $\sigma = \{v_{i_1}, \dots, v_{i_{\kappa+1}}\}$, $i_1 < \dots < i_{\kappa+1}$, and $\alpha \subset \sigma$ is its face. Then, $\sigma \setminus \alpha = \{v_{i_{\ell^*}}\}$ for some $\ell^* \in \{1, \dots, \kappa + 1\}$. Define the *natural parity* of σ with respect to its face α as $\text{nat}(\sigma, \alpha) := (-1)^{\ell^*+1}$. An *oriented* simplex σ further has an orientation $p_\sigma \in \{\pm 1\}$ which indicates whether its parity with its faces is the same as, or opposite to, its natural parity. When $p_\sigma = +1$, we say σ is in *natural orientation*. For example, a directed edge $e = (v_i, v_j)$ for $i < j$ is in natural orientation, while if $i > j$, $p_e = -1$. An oriented simplicial complex contains at most one orientation for any given simplex.

Given an oriented simplicial complex C , for each $\kappa \in \{0, 1, \dots, \kappa_{\max}\}$, the *boundary operator* is a linear operator $B_\kappa : X_{\kappa+1} \mapsto X_\kappa$, where for $\sigma \in C_{\kappa+1}$, $\alpha \in C_\kappa$, the corresponding matrix entries are $[B_\kappa]_{\alpha\sigma} = p_\sigma p_\alpha \text{nat}(\sigma, \alpha)$. Likewise, the *coboundary operator* for each $\kappa \in \{0, 1, \dots, \kappa_{\max}\}$ is just $B_\kappa^\top : X_\kappa \rightarrow X_{\kappa+1}$, the adjoint to B_κ . The entries of B_κ express *relative* orientation between simplex and face, and they are a natural way to construct functions taking local signed averages, according to adjacency in the simplicial complex.

2.2. Hodge Laplacian

The boundary operators just introduced represent *discrete differential operators* encoding the structure of κ -regions in a simplicial complex, and so can be building blocks towards a spectral analysis of functions on those regions. For analyzing functions on κ -simplices with $\kappa > 0$, we will construct operators based on the *Hodge Laplacian*, or κ -*Laplacian*. As in [15], the *combinatorial* κ -Laplacian is defined for κ -simplices as

$$L_\kappa := B_{\kappa-1}^\top B_{\kappa-1} + B_\kappa B_\kappa^\top . \quad (1)$$

Various forms of weighting and normalization are possible, with corresponding advantages and difficulties, and different interpretations of the resulting Hodge Laplacian's Fiedler vector, as explored in [29, Chap. 4]. In our numerical experiments, we choose the *symmetrically normalized, weighted* Hodge Laplacian, defined as in [14], as follows. For each $\kappa \in \{0, 1, \dots, \kappa_{\max}\}$, let D_κ refer to a diagonal matrix, whose diagonal entries contain an assignment of positive weights to each κ -simplex in C_κ .

One such choice, as in [14], is to set a simplex's weight as its degree, by taking $D_{\kappa+1} = I$, $\text{diag}(D_\kappa) = |B_\kappa| \text{diag}(D_{\kappa+1})$, and $\text{diag}(D_{\kappa-1}) = |B_{\kappa-1}| \text{diag}(D_\kappa)$, where $[[M]]_{\alpha\sigma} = |[M]_{\alpha\sigma}|$. Define the *normalized boundary matrix* $\mathcal{B}_\kappa := D_\kappa^{-1/2} B_\kappa D_{\kappa+1}^{1/2}$. Then the symmetrically normalized, weighted Hodge Laplacian is defined as

$$\mathcal{L}_\kappa := \mathcal{B}_{\kappa-1}^\top \mathcal{B}_{\kappa-1} + \mathcal{B}_\kappa \mathcal{B}_\kappa^\top . \quad (2)$$

Through the rest of this article, when we wish to refer to some variant of the Hodge Laplacian calculated on a κ -region R , without specifying a choice of normalization and/or weighting, we will use $\mathcal{L}(R)$. When $R = C_\kappa$, we simplify to $\mathcal{L} := \mathcal{L}(C_\kappa)$.

2.3. The κ -HGLET

The κ -HGLET is a generalization of the *Hierarchical Graph Laplacian Eigen Transform* (HGLET) [30] from functions on the nodes of a graph, to functions on the κ -simplices in a given simplicial complex [7]. The HGLET, in turn, can be viewed as a generalization of the Hierarchical Block Discrete Cosine Transform (HBDCT), which is generated by creating a hierarchical bipartition of the signal domain and computing the DCT of the local signal supported on each subdomain.

Let $\{\phi_{k,l}^j\}$ be the set of basis vectors in the κ -HGLET dictionary where j denotes the level of the partition (with $j = 0$ being the root), k indicates the partition within the level, and l indexes the elements within each partition in increasing frequency. Let C_k^j refer to the κ -region consisting of the support of partition k at level (or scale) j , and let $n_k^j := |C_k^j|$. Hence $C_0^0 = C_\kappa$ and $n_0^0 = |C_\kappa| =: n$.

In order to compute the transform, we first compute the complete set of eigenvectors $\{\phi_{0,l}^0\}_{l=0:n_0^0-1}$ of $\mathcal{L} = \mathcal{L}(C_0^0)$, and order them by nondecreasing eigenvalues. We then partition C_0^0 into two disjoint κ -regions C_0^1 and C_1^1 by forming the Fiedler vector of \mathcal{L} . We note that: 1) one can use any other bipartition methods; and 2) bipartitioning with the Fiedler vector in the κ -region setting requires additional steps vs. the graph setting, because of its rather intricate behaviors; see [7] for the details. We iterate the same procedure for C_0^1 and C_1^1 to generate the eigenvectors $\{\phi_{0,l}^1\}_{l=0:n_0^1-1}$ and $\{\phi_{1,l}^1\}_{l=0:n_1^1-1}$. Note that $n_0^1 + n_1^1 = n_0^0 = n$, and that all of the elements in $\{\phi_{0,l}^1\}$ are orthogonal to those in $\{\phi_{1,l}^1\}$ since their supports are disjoint. The set $\{\phi_{0,l}^1\}_{l=0:n_0^1-1} \cup \{\phi_{1,l}^1\}_{l=0:n_1^1-1}$ form an ONB for vectors in X_κ . From here, we apply this process recursively, generating an ONB for each level in the given hierarchical bipartition tree. If the hierarchical bipartition tree terminates at every region containing only a κ -simplex singleton, then the final level will simply be the standard basis of \mathbb{R}^n . Each level of the dictionary contains an ONB whose vectors have the support of roughly half the size of the previous level. There are roughly $(1.5)^n$ possible ONBs formed by selecting different covering sets of regions from the hierarchical bipartition tree. We also note that the computational cost of generating the entire dictionary is $\mathcal{O}(n^3)$. See [7] for the actual algorithm to generate the κ -HGLET on a given C_κ and further details.

2.4. The κ -GHWT

This basis dictionary is based on the *Generalized Haar-Walsh Transform* (GHWT) [8], which can itself be viewed as a generalization of the Haar-Walsh wavelet packets [31, Sec. 8.1]. This is formed by first generating a hierarchical bipartition tree of C_κ as for the κ -HGLET. We then work in a bottom-up manner, beginning with the finest level

$j = j_{\max}$ where each region only contains a single element that is the indicator vector of that region. We call them *scaling vectors* and label them as $\{\psi_{k,0}^{j_{\max}}\}_{k=0:n-1}$. For the next level $j = j_{\max} - 1$, we first assign a constant scaling vector for the support on each region. Then, for each region that contains two children in the partition tree, we form a *Haar vector* by subtracting the scaling vector of the child element with a higher index from that of the child element with a lower index. This procedure will form an ONB $\{\psi_{k,l}^{j_{\max}-1}\}_{k=0:K-1,l=0:l(k)-1}$ (where K is the number of κ -regions at level $j_{\max} - 1$ and $l(k) = 1$ or 2 depending on the region k) whose vectors have support of at most 2. For the level $j = j_{\max} - 2$, we begin by computing the scaling and Haar vectors as before. Next, for any region that contains three or more elements, we also compute *Walsh vectors* by adding and subtracting the Haar vectors of the children regions. From here, we form the rest of the dictionary recursively. A full description of this algorithm is given in [30] for the $\kappa = 0$ case and in [7] for the general case of $\kappa > 0$.

Note that like the κ -HGLET, each level of the dictionary forms an ONB, and at each level, basis vectors have the support of roughly half the size of the parent level. These basis vectors also have the same support as the corresponding κ -HGLET basis vectors (that is, $\text{supp}(\phi_{k,l}^j) = \text{supp}(\psi_{k,l}^j)$ for all j, k, l). However, the computational cost of computing the κ -GHWT is only $\mathcal{O}(n \log n)$.

3. Multiscale Hodge Scattering Transform

Let the κ -HGLET or κ -GHWT dictionary vectors be arranged as $\Phi^J := \{\Phi^j\}_{j=0}^J$ where each Φ^j is an ONB at scale (or level) j with $j = 0$ being the finest scale basis, composed of delta functions. *Note that this definition of the scale parameter j is the opposite of that used in the previous sections.* In general, we have $j_{\max} + 1 \approx \log_2 n + 1$ different levels given by the hierarchical bipartition scheme, but in practice, the features extracted by large j values are not very descriptive [4]. Hence, we typically use the first $J + 1 (\leq j_{\max} + 1)$ levels.

Let $\mathbf{f} \in X_\kappa$ and let $[\mathbf{f}]_i$ denote \mathbf{f} evaluated at simplex i . In addition, let us write $|\mathbf{f}|^q := (|[\mathbf{f}]_1|^q, \dots, |[\mathbf{f}]_n|^q) \in \mathbb{R}^n$ for $q \in \mathbb{N}$. We propose to compute the q th moment up to some maximum $Q \in \mathbb{N}$ of the 0th-order and 1st-order scattering coefficients:

$$S^0(q)\mathbf{f} := \frac{1}{n} \sum_{i=1}^n [\mathbf{f}]_i^q, \quad S^1(q, j)\mathbf{f} := \frac{1}{n} \sum_{i=1}^n [|\Phi^j \mathbf{f}|^q]_i, \quad 0 \leq j \leq J; 1 \leq q \leq Q, \quad (3)$$

and the 2nd-order scattering coefficients:

$$S^2(q, j, j')\mathbf{f} := \frac{1}{n} \sum_{i=1}^n \left[\left| \Phi^{j'} |\Phi^j \mathbf{f}| \right|^q \right]_i, \quad 0 \leq j < j' \leq J, \quad 1 \leq q \leq Q. \quad (4)$$

And higher-order moments can be computed in a similar manner:

$$S^m(q, j^{(1)}, \dots, j^{(m)})\mathbf{f} := \frac{1}{n} \sum_{i=1}^n \left[\left| \Phi^{j^{(m)}} \left| \Phi^{j^{(m-1)}} \left| \dots \left| \Phi^{j^{(1)}} \mathbf{f} \right| \dots \right| \right|^q \right]_i, \quad (5)$$

where $0 \leq j^{(1)} < \dots < j^{(m)} \leq J$. However, due to the combinatorial blow-up in the number of features at each order, it is rare to use more than 2nd or 3rd-order features.

Note that the m th order features are computed by applying a multiplication with the appropriate (sparse) weight Φ^j then applying a pointwise nonlinearity to $(m-1)$ st-order features. Further, as we later find in our numerical experiments, high-order moments ($Q > 4$) are not very useful in practice due to their instability [2, 4, 25]. By defining the operator $\hat{S}^1(j, q)\mathbf{f} := |\Phi^j \mathbf{f}|^q$, which maps $\mathbf{f} \in \mathbb{R}^n$ to $\mathbb{R}_{\geq 0}^n$, we can also rewrite the higher-order features Eq. (5) in a more comprehensible manner as:

$$S^m(q, j^{(1)}, \dots, j^{(m)})\mathbf{f} = S^1(q, j^{(m)})\hat{S}^1(1, j^{(m-1)})\dots\hat{S}^1(1, j^{(1)})\mathbf{f} \quad (6)$$

This behavior mimics the architecture of convolutional neural networks (with fixed weights) and has been studied extensively [1]. However, unlike traditional feed-forward networks, rather than only considering the features extracted at end of the cascade of linear and nonlinear layers, we concatenate the representation extracted at each layer for downstream analysis. In general, we refer to the process of extracting these features as the *Multiscale Hodge Scattering Transform* (MHST). Later we will analyze these features with relatively simple machine learning models such as support vector machines (SVMs) and logistic regression models (LRMs). When working with such models with learnable parameters in concert with these deterministic features, we refer to it as the *Multiscale Hodge Scattering Network* (MHSN).

3.1. Local Pooling

In general, we can gather all of the moments $\leq Q$ and of orders $\leq M$ to have a total of $Q \sum_{k=0}^M \binom{J+1}{k}$ features for a given signal. The summations from $i = 1$ to $i = n$ in (3)–(5) can be viewed as *global* pooling operations. In situations where permutation invariance is not required (i.e., all signals are defined on a fixed complex with known node ordering), however, we can omit these sums, i.e., no pooling is done. As a result, we are left with $Qn \sum_{k=0}^M \binom{J+1}{k}$ features for each signal. We can also generate intermediate features between these two extremes: retain sums over each region k at level j instead of not summing at all or summing all the regions of level j in (3)–(5). This can be viewed as *local* pooling operations and results in a tuple of features rather than a single value as in the original scattering transform. This is similar to the windowed scattering transforms recently proposed by [25], but here we leverage the multiscale decomposition provided by the hierarchical partition tree to avoid introducing a new user parameter to determine the window size. In the case of these local pools, we replace the normalization factor in the averaging operation with the number of elements in the local pool rather than the number in the entire simplex as defined in Eq. (7). This gives us a total of $Q \sum_{j=0}^M K^j \binom{J+1}{j}$ features, where K^j is the number of local sums taken in the j th level, i.e., the number of regions at scale j .

We denote these transforms as S_j^m where j denotes the level at which the sum has taken place. So $S_{j_{\max}}^m = S^m$ indicated the standard max-pooling-like scheme as defined by [2, 4]. Then S_0^m denotes the transform without any sums while S_2^m denotes the transform with local pools determined by the third level (i.e., $j = 2$) of the partition tree. In general we have:

$$S_j^m(q, j^{(1)}, \dots, j^{(m)})\mathbf{f} := \left\{ \frac{1}{n_k^j} \sum_{i \in C_k^j} \left[\left| \Phi^{j^{(m)}} \right| \left| \Phi^{j^{(m-1)}} \right| \dots \left| \Phi^{j^{(1)}} \mathbf{f} \right| \dots \right]_i^q \right\}_{k=0}^{K^j-1} \quad (7)$$

Note that the subscript j indicates where the final averaging has taken place whereas $j^{(m)}$ indicates the index of the basis elements used to compute the feature.

4. Theoretical Analysis of Multiscale Hodge Scattering Transforms

In this section we establish approximation properties of the multiscale basis dictionaries, then use these results to detail the continuity, invariance and equivalence properties of the MHSNs which make them desirable for signal and domain classification problems. For notational convenience, we let $S = S^1$ and only consider the first order transform in our formal proofs. However, since $S^m \mathbf{f}$ can be thought of as applying S^1 to the transform $S_0^{m-1} \mathbf{f}$, all of the proofs can be trivially generalized to the S^m case.

First, for singleton κ -elements σ and τ of C_κ , and signal \mathbf{f} , we define a distance function and then the associated Hölder semi-norm as the number of elements in the smallest partition in the tree that constrains both elements, formally we have:

$$d(\sigma, \tau) := \min \left\{ n_k^j \mid \sigma, \tau \in C_k^j \right\}, \quad C_H(\mathbf{f}) := \sup_{\sigma \neq \tau} \frac{|[\mathbf{f}]_\sigma - [\mathbf{f}]_\tau|}{d(\sigma, \tau)^\alpha}$$

where α is a constant in $(0, 1]$. With these definitions, the dictionary coefficient decay and approximation results of [32, 6] for the GHWT and HGLET can be applied to the κ -GHWT and κ -HGLET bases as detailed further in [7].

Theorem 1 (Fast Decay of Multiscale Coefficients). *For a simplicial complex C equipped with a hierarchical bipartition tree, suppose that a signal \mathbf{f} is Hölder continuous with exponent α and constant $C_H(\mathbf{f})$. Then the coefficients with $l \geq 1$ for the κ -HGLET $(c_{k,l}^j)$ and κ -GHWT $(d_{k,l}^j)$ satisfy:*

$$|c_{k,l}^j| \leq C_H(\mathbf{f}) (n_k^j)^{\alpha + \frac{1}{2}}, \quad |d_{k,l}^j| \leq C_H(\mathbf{f}) (n_k^j)^{\alpha + \frac{1}{2}}$$

Proof. See Theorem 3.1 of [6]. □

Theorem 2 (Approximation Power of Multiscale Bases). *For a fixed ONB $\{\phi_l\}_{l=0}^{n-1}$ and a parameter $0 < \rho < 2$, then*

$$\|\mathbf{f} - P_m \mathbf{f}\|_2 \leq \frac{|\mathbf{f}|_\rho}{m^\beta}.$$

where P_m is the best nonlinear m -term approximation in the basis $\{\phi_l\}_{l=0}^{n-1}$, $\beta = \frac{1}{\rho} - \frac{1}{2}$ and $|\mathbf{f}|_\rho$ is defined as $|\mathbf{f}|_\rho := \left(\sum_{l=0}^{n-1} |\langle \mathbf{f}, \phi_l \rangle|^\rho \right)^{\frac{1}{\rho}}$

Proof. See Theorem 3.2 of [6] and Theorem 6.3 of [32]. □

Next we establish bounds on the coefficients generated by the multiscale basis. Let \mathcal{W} indicate the matrix formed by stacking a multiscale basis into a $(J+1)n \times n$ matrix where the j th $n \times n$ block is the j th-level ONB. Next we define a weighted inner product and the associated norm for signals in X_κ as:

$$\langle \mathbf{f}, \mathbf{g} \rangle_w := \sum_{\sigma \in C_\kappa} [\mathbf{f}]_\sigma [\mathbf{g}]_\sigma [\mathbf{w}]_\sigma \quad \text{and} \quad \|\mathbf{f}\|_w := \sqrt{\langle \mathbf{f}, \mathbf{f} \rangle_w}.$$

In practice, we can often use $\mathbf{w} \equiv \mathbf{1}$, but for some applications more exotic norms, such as those that consider the volume of each face, may be useful.

Remark 1 (Tight Frames). *Let $\mathbf{f} \in X_\kappa$, and $\|\cdot\|_w$ indicate the ℓ^2 -norm with respect to the metric w . Then we have:*

$$\|\mathbf{f}\|_w^2 \leq \|\mathcal{W}\mathbf{f}\|_w^2 = (J+1)\|\mathbf{f}\|_w^2$$

This remark is clearly true since \mathcal{W} is simply a collection of $J+1$ orthogonal matrices, and orthogonal transforms preserve the ℓ^2 -norm. Although trivial, this fact will be vital for later proofs. Next we show that the MHST is a non-expansive operation. This allows for powerful nonlinear analysis properties [33] which we detail later.

Theorem 3 (Non-expansive Operation). *Let S be the MHST with global pooling formed by the multiscale basis dictionary \mathcal{W} as defined above in (3)–(5), acting on the metric space \mathcal{W} . Then we have:*

$$\|S\mathbf{f}_1 - S\mathbf{f}_2\|_w \leq \|\mathbf{f}_1 - \mathbf{f}_2\|_w$$

Moreover, let S_j indicate the transforms with local pooling as described in Section 3.1, then for all $0 \leq j \leq J$ we have:

$$\|S_j\mathbf{f}_1 - S_j\mathbf{f}_2\|_w \leq \|\mathbf{f}_1 - \mathbf{f}_2\|_w$$

Proof. To show that the MHST is non-expansive, we will show that each layer is non-expansive. Since the entire transform is defined by a cascade of these layers (with modulus operations taken between the layers), it will also be non-expansive. Then:

$$\begin{aligned} S^1(q, j)(\mathbf{f}_1 - \mathbf{f}_2) &= \frac{1}{n} \sum_{i=1}^n |[\Phi^j(\mathbf{f}_1 - \mathbf{f}_2)]_i|^q \\ &\leq \left| \frac{1}{n} \sum_{i=1}^n |[\Phi^j \mathbf{f}_1]_i|^q - \frac{1}{n} \sum_{i=1}^n |[\Phi^j \mathbf{f}_2]_i|^q \right| = |S^1(q, j)\mathbf{f}_1 - S^1(q, j)\mathbf{f}_2| \end{aligned} \quad (8)$$

Since this inequality holds for each q and j , it is clear that taking the w -norm over the whole collection of features $S^1\mathbf{f}$ will also hold. Then, since each order of the transform features can be formed by applying S^1 to the previous order we have: $\|S\mathbf{f}_1 - S\mathbf{f}_2\|_w \leq \|\mathbf{f}_1 - \mathbf{f}_2\|_w$. The proof for the local summation follows exactly as above. \square

Next we show that our networks are invariant under group operations which preserve the inner product $\langle \cdot, \cdot \rangle_w$, such as permutations of the κ -simplices. That is, relabeling indices of the elements of C_κ does not affect the output of the transform. For example, given a signal \mathbf{f} defined on the triangular faces of a simplex, the indexing of the triangles does not effect the globally pooled transform and permuting this indexing results in an equivalent permutation of the non-pooled signal. This theorem is analogous to Theorem 3 in [25] and Proposition 4.1 in [34], but generalizes to any κ , rather than strictly to the nodes ($\kappa=0$ case).

Theorem 4 (Invariance and Equivariance). *Suppose \mathcal{G} is a group of transforms on the elements of C_κ (e.g., permutations of the κ -simplices). Furthermore, given any $\xi \in \mathcal{G}$, let $V_\xi : C_\kappa \rightarrow C_\kappa$ denote the operator $V_\xi\mathbf{f} = \mathbf{f} \circ \xi$ induced by ξ and $S^{[\xi]}$ the analogous transform on $C_\kappa^{[\xi]}$, which is the permuted version of C_κ . Then both of the following hold:*

$$S^{[\xi]}V_\xi\mathbf{f} = S\mathbf{f} \quad \text{and} \quad S_j^{[\xi]}V_\xi\mathbf{f} = S_j\mathbf{f} \quad (9)$$

for all $\xi \in \mathcal{G}$, $\mathbf{f} \in \mathbb{R}^n$ and $0 \leq j \leq J$.

Proof. As with the previous proof we will show that this holds for an arbitrary layer, and since the entire transform is formed from a cascade of these layers, it will also have this property. First, denote $\mathcal{L}_\xi = V_\xi \circ \mathcal{L} \circ V_\xi^{-1}$ where \mathcal{L} is an appropriate version of the κ -Laplacian for C_κ . It is immediately clear that if ϕ is an eigenvector of \mathcal{L} with $\mathcal{L}\phi = \lambda\phi$ then $V_\xi\phi$ is an eigenvector of \mathcal{L}_ξ , i.e., $\mathcal{L}_\xi V_\xi\phi = \lambda V_\xi\phi$ since

$$\mathcal{L}_\xi V_\xi = V_\xi \circ \mathcal{L} \circ V_\xi^{-1} \circ V_\xi = V_\xi \circ \mathcal{L} \quad (10)$$

Then Since \mathcal{G} preserves the inner product on \mathcal{W} , it is clear that $V_\xi\Phi := \Phi_\xi$ is an ONB for \mathcal{W}_ξ whose atoms are the bases Φ_ξ formed from eigenvectors of \mathcal{L}_ξ , where $\Phi_\xi = V_\xi\Phi V_\xi^{-1}$

Then for arbitrary input f we have:

$$S^{[\xi]} V_\xi \mathbf{f} = \frac{1}{n} \sum_{i=1}^n |[\Phi_\xi V_\xi \mathbf{f}]_i| = \frac{1}{n} \sum_{i=1}^n |[V_\xi \Phi \mathbf{f}]_i| = \frac{1}{n} \sum_{i=1}^n |[\Phi \mathbf{f}]_i| = S \mathbf{f} \quad (11)$$

The proof for the local summation follows exactly as above. \square

5. Signal Classification

We first demonstrate the effectiveness of our MHSNs with the article category classification problem using the *Science News* database [35, 36]. We do not claim state-of-the-art results for this problem, but rather use it to illustrate the advantages of analyzing signals via higher-dimensional simplices. We also show how locally-pooled networks can shatter problems in which traditional globally-pooled scattering networks fail to differentiate between classes. The Science News dataset contains 1042 scientific news articles classified into eight fields: Anthropology, Astronomy; Behavioral Sciences; Earth Sciences; Life Sciences; Math/CS; Medicine; Physics. Each article is tagged with keywords from a pool of 1133 words selected by the database curators. We determine a simplicial complex from these keywords by computing their `word2vec` [37] embeddings based on Google’s publicly available pre-trained model [38]. We generate a symmetric k -nearest neighbor graph of the embedded words and then generate κ -simplices of the graph. Therefore, a κ -simplex in this keyword graph corresponds to κ -face, which represents a combination of $\kappa + 1$ words.

Next, we define representations of each article as a signal in each X_κ as follows. First, for $\kappa = 0$ (i.e., a node-valued signal), we define the signal \mathbf{f}_0 to be one on the nodes representing their keywords and zero elsewhere. For $\kappa \geq 1$ we define the signal \mathbf{f}_κ to be the simplex-wise average of the \mathbf{f}_0 signal. That is,

$$[\mathbf{f}_0]_i = \begin{cases} 1 & \text{if keyword } i \text{ occurs} \\ 0 & \text{Otherwise} \end{cases} ; \quad [\mathbf{f}_\kappa]_i = \frac{1}{\kappa + 1} \sum_{\substack{l \in V(\sigma_i) \\ \sigma_i \in C_\kappa}} [\mathbf{f}_0]_l, \quad (12)$$

where $V(\sigma_i)$ represents the set of nodes forming the i th simplex $\sigma_i \in C_\kappa$. Note that these signals are highly localized since the keywords are connected through a symmetrized k NN graph, and the higher-order signals are built from the adjacency of the resulting complex. To showcase the robustness of our approach, we report results using both $k = 5$ and $k = 10$ nearest neighbor graphs.

Tables 1 and 2 compare the performance of our proposed methods with the other simpler methods, i.e., the raw expansion coefficients of the signals relative to the standard ONBs (Delta; Fourier) or the dictionaries (Diffusion; HGLET; GHWT). The parameters for the feature computations were set as $(J, M, Q) = (5, 3, 4)$. For each κ , we performed the five-fold cross-validation, i.e., we randomly split these 1042 signals into 80% training and 20% test sets and repeat the experiment 5 times with different train/test splits. In every case we use the ℓ^2 -regularized LRM provided by `scikit-learn` [39] without any additional hyperparameter tuning to compute the classification.

Several observations are in order. First, the traditional, globally-pooled scattering networks mostly fail on this task regardless of the wavelet dictionary employed. Since the number of nonzero entries in each signal is similar and therefore the ℓ^1 -norms are also similar, global-pooling schemes fail to capture the keyword information (i.e., indices of nonzero entries) in a way that differentiates between the classes and consequently do not produce statistically significant results. The non-pooled features often provide the highest performance, which is not surprising since there are many more features and learnable parameters than the networks with pooling. However, the locally-pooled features almost always perform on par with the non-pooled features. For both the 5 and 10 nearest neighbor graphs, the best overall results are achieved by the κ , which has the largest number of elements. Similarly, the 10-nearest neighbor graph performs better than the 5-nearest neighbor graphs at the cost of larger n .

We also observe that the networks based on κ -HGLET and κ -GHWT generally outperform those based on Diffusion Wavelets. This is likely due to the highly localized and piecewise constant nature of the input signals, which are well-approximated by these dictionaries [7]. In the next section, where the signals are not localized, we do not observe this difference.

Knn = 5	n	Delta	Fourier	Diffusion			HGLET				GHWT			
		Basis	Basis	Dict.	GP	NP	Dict.	GP	LP	NP	Dict.	GP	LP	NP
$\kappa=0$	1133	33.971	33.971	86.603	31.579	86.603	81.818	31.579	86.603	86.603	80.861	31.579	85.646	86.124
$\kappa=1$	3273	55.502	78.947	<u>85.646</u>	31.579	<u>85.646</u>	86.124	31.579	86.124	<u>85.646</u>	85.603	31.579	85.646	85.646
$\kappa=2$	1294	55.502	49.761	83.732	31.579	83.732	83.254	31.579	84.211	83.732	83.732	31.579	83.254	83.254
$\kappa=3$	227	31.579	31.579	78.947	31.579	78.947	51.675	31.579	78.469	78.947	51.196	31.579	78.469	78.947
$\kappa=4$	16	31.579	31.579	55.981	31.100	55.981	32.057	31.100	55.981	55.981	32.057	37.799	55.502	54.067

Table 1: Article category classification accuracy for 5-NN graph of the Science News dataset for different simplex degrees. Dict. implies that the SVM is trained solely on the dictionary coefficients while GP, LP, NP imply scattering networks with global, local, and no pooling, respectively. The best performer for each κ is indicated in bold while the underlined bold numbers are the best among all κ 's.

6. Domain Classification

Another vital application of geometric scattering networks and graph neural networks (GNNs) is graph (and simplex) classification. Broadly speaking, this problem consists of predicting a label of a social or chemical graph based on a training set of similar graphs with different configurations (i.e., different numbers of nodes and edges). For example, in the COLLAB dataset [52], each graph represents a network of coauthors of a scientific paper. Since the size of the graphs varies greatly within these datasets,

$\kappa_{nn} = 10$	n	Delta		Fourier			Diffusion				HGLET				GHWT			
		Basis	Basis	Dict.	GP	NP	Dict.	GP	LP	NP	Dict.	GP	LP	NP	Dict.	GP	LP	NP
$\kappa=0$	1133	35.238	35.238	60.952	32.381	87.619	81.905	32.381	88.571	87.619	80.952	32.381	87.619	87.619	80.952	32.381	87.619	87.619
$\kappa=1$	6890	81.905	81.905	86.667	32.381	86.667	85.714	32.381	89.524	86.667	85.714	32.381	89.524	89.524	85.714	32.381	89.524	89.524
$\kappa=2$	7243	76.19	76.19	86.667	32.381	88.571	85.714	32.381	88.571	88.571	88.571	32.381	89.524	88.571	88.571	32.381	89.524	88.571
$\kappa=3$	4179	69.524	69.524	74.286	33.333	86.667	86.667	33.333	86.667	86.667	86.667	33.333	86.667	86.667	86.667	33.333	86.667	86.667
$\kappa=4$	1740	45.714	45.714	68.571	35.238	81.905	73.333	35.238	81.905	81.905	81.905	33.333	81.905	81.905	33.333	81.905	81.905	81.905
$\kappa=5$	560	33.333	33.333	39.048	34.286	73.333	60.952	33.333	73.333	73.333	60.952	34.286	73.333	73.333	60.952	34.286	73.333	73.333
$\kappa=6$	98	32.381	32.381	32.381	34.286	62.857	39.048	35.238	62.857	62.857	62.857	35.238	62.857	62.857	35.238	62.857	62.857	60.952

Table 2: Article category classification accuracy for 10-NN graph of the Science News dataset for different simplex degrees. Dict. implies that the SVM is trained solely on the dictionary coefficients while GP, LP, NP imply scattering networks with global, local, and no pooling, respectively. The best performer for each κ is indicated in bold while the underlined bold numbers are the best among all κ 's.

we employ only the global-pooling version of our MHSN, akin to the previous efforts reported in [4, 25], which were based on geometric scattering methods.

We compute permutation-invariant input features based only on topological information obtainable from the boundary matrices. Since many of the graphs are too small to contain high-degree simplices, we only consider node and edge-based features and transforms. Following the methodology developed in [4], we set $(J, M, Q) = (4, 2, 4)$. For the node signals, we first compute the eccentricity and clustering coefficient [?, Sec. 1.2] of each node. For each node signal, the number of parameters (MHST coefficients) are 64 via the formula $Q \sum_{k=0}^M \binom{J+1}{k}$, hence 128 parameters after concatenating them. For the edge signals, we use the average of the eccentricities of the head and tail nodes of each edge and the number of non-zero off-diagonal terms in the combinatorial Hodge-Laplacian (each such term corresponds to a 1-adjacent edge [29, Sec. 4.1]).

For each domain classification problem we train three models: 1) using 128 node features; 2) using 128 edge features; and 3) using 256 combined features. We then employ a simple SVM with Gaussian radial basis functions to classify the features. Moreover, we tune the hyperparameters controlling the strength of the ℓ^2 -regularization and the kernel coefficients via the cross-validation scheme presented in [4] using the same search space and validation indexes.

We compare these results with those obtained by the geometric scattering network (with Diffusion Wavelets) using SVM (GS-SVM) as well as several popular GNN models including the graph convolution network (GCN) [40], universal graph transform (UGT) [41], dynamic graph CNN (DGCNN) [42], graph attention network (GAT) [43], and graph feature network (GFN) [44]. For each competing method, we reproduce the results in the significant figures reported in their original publications; we report to 2 decimal places for our method. More information on the benchmark datasets can be found in Appendix A. We remark that, as of this article's writing, this collection of networks achieves state-of-the-art results on these datasets according to the Papers with Code Leaderboards [45]. Further details on these datasets and their associated classification problems are presented in Appendix A and the references therein.

Although our MHSNs do not achieve state-of-the-art results on these datasets, they are very competitive with *only a small fraction of the learnable parameters*. Moreover, the number of learnable parameters in our models is not tied to the graph size and depends only on the order of the scattering M and the number of moments Q computed. For example, Table 4 compares our methods with the UGT and the GFN, which are the state-of-the-art methods for various graph classification problems. These methods

Graph	Node Scattering	Edge Scattering	Combo	GS-SVM	GCN	UGT	DGCNN	GAT	GFN
COLLAB	70.84	78.34	80.39	79.94	79.00	77.84	73.76	75.80	81.50
DD	60.67	68.73	72.71	-	-	80.23	79.37	-	79.37
IMDB-B	72.70	70.60	73.10	71.20	74.00	77.04	70.03	70.50	73.40
IMDB-M	44.40	47.13	49.68	48.73	51.90	53.60	47.83	47.8	51.80
MUTAG	85.78	86.31	85.78	83.50	85.60	80.23	79.37	89.40	85.83
PROTEINS	73.57	73.04	75.35	74.11	76.00	78.53	75.54	74.70	76.46
PTC	62.85	67.71	68.28	63.94	64.20	69.63	58.59	66.70	66.60

Table 3: Graph classification accuracy on seven datasets. The best performer for each dataset is indicated in bold.

each require more than half a million parameters for some cases (867K for UGT) to achieve results similar to ours, requiring only 256 parameters to learn. As a result, our MHSNs can be implemented and trained on a consumer-level laptop, whereas many of these competing GNNs require specialized hardware.

Graph	Hodge Scattering + SVM		UGT		GFN	
	Accuracy	# Parameters	Accuracy	# Parameters	Accuracy	# Parameters
COLLAB	80.39	256	77.84	866,746	81.50	68,754
DD	72.71	256	80.23	76,928	79.37	68,754
IMDB-B	73.10	256	77.04	55,508	73.40	68,754
IMDB-M	49.68	256	53.60	48,698	51.80	68,818
MUTAG	85.78	256	80.23	4,178	85.83	65,618
PROTEINS	75.35	256	78.53	1,878	76.46	65,618
PTC	68.28	256	69.63	12,038	66.60	65,618

Table 4: Comparison of MHSN and state of the art graph classification networks in accuracy and number of learnable parameters

7. Molecular Dynamics

Our MHSNs can also be used for regression problems where the goal is to predict a continuous property of a simplicial complex (or simply a graph) based on a set of observations of the complex under various conditions. Therefore, they are quite suitable for learning molecular dynamics, particularly the potential energy surface of a molecule, given a few registrations of the molecule and its energies. The Revised Molecular Dynamics 17 (rMD17 dataset) [46] contains 100,000 structures and associated energies of various molecules. However, these structures are taken from a molecular dynamics simulation, i.e., time series data, which is not independent and identically distributed. To overcome this, instead of using the entire dataset, we use five sets of molecule snapshots and the associated potential energies. Each of these sets consists of 1,000 snapshot/energy pairs and is grouped into 800 training and 200 test samples selected by the authors of the dataset [46].

We extract a rich set of features for each structure (i.e., a pose or conformation of a molecule) using our MHSNs (without pooling) and then employ a support vector regression (SVR) method with Gaussian radial basis functions to approximate and predict the energy. More specifically, for each molecule, we first compute the average position of each atom across the training set. Then, using these positions, we create a k NN-graph (with $k = 5$) as a template simplicial complex. Note that by using this simplicial complex, rather than the molecular-bond graph, we can better capture the

geometric information in the pose of the molecule as detailed in [47, 48]. Unlike the domain classification problems in Section 6, the geometry of the simplicial complex is fixed, so rather than use its geometrically-invariant descriptors, we need to begin with signals that encode the position information of molecules. We then generate the node and edge signals of both training and test sets as follows. First we compute the Euclidean distance matrix of (i.e the Gram matrix of the point-cloud, measured in the Euclidean distance) the node coordinates of each snapshot and assign the corresponding column vector of the distance matrix as its node features. This generates a number-of-atoms-dimensional node signal for each node, for each snapshot. For an edge signal, we extract edge lengths from the above distance matrix and create a diagonal matrix of edge lengths. Then, we assign the corresponding column vector of this diagonal matrix as its edge features. As with the node-based signal, this gives us number-of-edges-dimensional signal to input into our MHSN. For this experiment we use $(J, M, Q) = (4, 2, 3)$. We do not use simplices of dimension $\kappa > 1$ and not set $J > 4$ and $Q > 3$ because the molecules are too small.

Table 5 shows our results for aspirin (21 atoms) and paracetamol (20 atoms) molecules. We compare our MHSNs with several state-of-the-art GNN approaches designed specifically for processing molecular dynamics, including SchNet [47], PaiNN [49], and two variants of Special Orthogonal Networks (SO3Nets) [50, 48]. We report both the mean absolute error (MAE) and root mean square error (RMSE) of the energy prediction, which are the standard metrics in the computational chemistry literature. Our MHSNs perform competitively with these approaches while employing roughly 1% as many learnable parameters as the competing methods. Additionally, we again observe that our edge-based analysis outperforms the node-based analysis. This demonstrates that higher-dimensional simplex analysis can be more powerful than node-only approaches, even in cases where the underlying graph may not have many higher-dimensional structures.

Feature Type	Diffusion+SVR			HGLET+SVR			GHWT+SVR			SchNet	PaiNN	SO3Net I	SO3Net II
	Node	Edge	Both	Node	Edge	Both	Node	Edge	Both				
Aspirin													
MAE	4.856	3.132	3.267	4.884	3.135	3.285	4.928	3.075	3.225	13.5	3.8	3.8	2.6
RMSE	6.181	4.144	4.314	6.215	4.129	4.407	6.213	4.123	4.316	18.3	5.9	5.7	3.8
# Parameters	924	3784	4708	924	3784	4708	924	3784	4708	~ 432k	~ 341k	~ 283k	~ 341k
Paracetamol													
MAE	4.609	2.715	2.795	4.723	2.643	2.710	4.748	2.624	2.699	8.4	2.1	2.2	1.4
RMSE	5.860	3.418	4.116	5.964	3.338	3.424	5.961	3.299	3.408	11.2	2.9	3.0	1.9
# Parameters	924	3784	4444	924	3784	4444	924	3784	4444	~432k	~ 341k	~283k	~341k

Table 5: Comparison of the performance of our MHSNs and the other state-of-the-art GNNs for potential energy prediction. We report the accuracy via MAE and RMSE as well as the number of trainable parameters in each network.

8. Conclusion

In this article, we proposed the *Multiscale Hodge Scattering Transforms/Networks* (MHSTs/MHSNs) for robust feature extraction from signals on simplicial complexes that can be used in classification and regression problems, fully utilizing our multiscale basis dictionaries on such simplicial complexes, i.e., κ -HGLET and κ -GHWT dictionaries. Our MHSTs/MHSNs also have pooling options for the scattering transform

outputs: no-pooling; local-pooling; and global-pooling. Such options allow our tools to apply for various classification and regression problems on simplicial complexes ranging from classification of signals recorded on simplicial complexes to classification of type of simplicial complexes (i.e., domain classification problems) to regression of potential energies in molecular dynamics. We demonstrated that MHSNs provide comparable results with those by the state-of-the-art GNNs with up to a two-order of magnitude reduction in number of learnable parameters. We strongly believe that our success here comes from the structure and organization of our multiscale basis dictionaries that are conveniently arranged in terms of scales and locations, which are suitable and quite amenable for generating scattering transform coefficients.

We plan to investigate how we can interpret the MHST coefficients that are identified as important by classification methods such as the LRMs. Because of the nonlinearities used in the MHSTs, converting the MHST coefficients to the features in the primal/original domain is difficult. Along this direction, we plan to examine the optimization method proposed by Weber [51, Chap. 4], which synthesizes an input signal that generates the significant scattering transform coefficients at the specified coefficient indices. In a related line of research, we will explore how the MHST coefficients can be used to identify important relationships within graphs that can be used to narrow the training space of various attention mechanisms/graph transformers for large-scale problems.

Acknowledgments

This research was partially supported by the US National Science Foundation grants DMS-1912747 and CCF-1934568 as well as the US Office of Naval Research grant N00014-20-1-2381. N. S. also thanks Stéphane Mallat and Gabriel Peyré for their hospitality and support during his sabbatical stay (Oct. 2021–Jan. 2022) at the Centre Sciences des Données, Ecole Normale Supérieure (Ulm).

Appendix A. Description of Domain Classification Datasets

Google COLLAB. [52] A collaboration dataset of 5K scientific papers represented as graphs. The goal is to predict which of three subfields a paper belongs to given its authors. The average number of nodes of these graphs is 45 while the number of nodes in the smallest graph is 32 and that of the largest graph is 492.

DD. [53] A dataset of 1178 molecular graphs of medium to large size. The goal of the classification problem is to predict whether the protein is enzyme or not. The average number of nodes is 285 while the number of nodes of the smallest graph is 30 and that of the largest graph is 5748.

IMDB-B and IMDB-M. [52] A pair of two datasets representing collaboration within popular movies from the Internet Movie Database with 1K (IMDB-B) and 1.5k (IMDB-M) graphs. Each graph represents members of cast and the goal is to predict the genre (Action/Romance for IMDB-B and Comedy/Romance/Sci-Fi of IMDB-M). The average, the smallest, and the largest number of nodes in IMDB-B are 20, 12, and 136 while those in IMDB-M are 13, 7, and 89.

MUTAG. [54] A dataset of 188 molecular graphs representing mutagenic aromatic and heteroaromatic nitro compound. The dataset contains node-based features (detailing atom type), but we use only the adjacency matrix for our classification tests as in [4]. The binary classification goal is to predict whether or not a molecule (graph) has a mutagenic effect on bacterium. The average number of nodes of these graphs is 18 while the number of nodes of the smallest graph is 10 and that of the largest graph is 28.

Proteins. [55] A dataset of 1113 molecular graphs. The goal of the classification problem is to predict whether the protein is enzyme or not. The task here is the same as in the DD dataset, but the molecules are both smaller and more similar to each other (see [55] for details). The average number of nodes is 39 while the number of nodes of the smallest graph is 4 and that of the largest graph is 620.

PTC. [56] A dataset of 344 molecular graphs. The goal is to predict whether or not the compound is known to be carcinogenic in rats. The average number of nodes of these graphs is 26 while the number of nodes of the smallest graph is 6 and that of the largest graph is 109.

References

- [1] S. Mallat, Group invariant scattering, *Comm. Pure Appl. Math.* 65 (10) (2012) 1331–1398.
- [2] J. Bruna, S. Mallat, Invariant scattering convolution networks, *IEEE Trans. Pattern Anal. Machine Intell.* 35 (8) (2013) 1872–1886.
- [3] W. H. Chak, N. Saito, Monogenic wavelet scattering network for texture image classification, *JSIAM Lett.* 15 (2023) 21–24.
- [4] F. Gao, G. Wolf, M. Hirn, Geometric scattering for graph data analysis, in: *International Conference on Machine Learning*, PMLR, 2019, pp. 2122–2131.
- [5] C. R. Qi, H. Su, K. Mo, L. J. Guibas, Pointnet: Deep learning on point sets for 3D classification and segmentation, in: *Proceedings of the IEEE Conference on Computer Vision and Pattern Recognition*, 2017, pp. 652–660.
- [6] J. Irion, N. Saito, Efficient approximation and denoising of graph signals using the multiscale basis dictionaries, *IEEE Trans. Signal Inform. Process. Netw.* 3 (3) (2017) 607–616.
- [7] N. Saito, S. C. Schonsheck, E. Shvarts, Multiscale transforms for signals on simplicial complexes, *Sampl. Theory Signal Process. Data Anal.* To appear; available as arXiv:2301.02136 [cs.SI] (2023).
- [8] J. Irion, N. Saito, The generalized Haar-Walsh transform, in: *2014 IEEE Workshop on Statistical Signal Processing (SSP)*, IEEE, 2014, pp. 472–475.
- [9] R. R. Coifman, M. Maggioni, Diffusion wavelets, *Appl. Comput. Harmon. Anal.* 21 (1) (2006) 53–94.

- [10] G. Carlsson, Topology and data, *Bull. Amer. Math. Soc.* 46 (2) (2009) 255–308.
- [11] D. I. Shuman, S. K. Narang, P. Frossard, A. Ortega, P. Vandergheynst, The emerging field of signal processing on graphs: Extending high-dimensional data analysis to networks and other irregular domains, *IEEE Signal Process. Mag.* 30 (3) (2013) 83–98.
- [12] C. Giusti, R. Ghrist, D. S. Bassett, Two’s company, three (or more) is a simplex, *J. Comput. Neurosci.* 41 (1) (2016) 1–14.
- [13] S. Barbarossa, S. Sardellitti, Topological signal processing over simplicial complexes, *IEEE Trans. Signal Process.* 68 (2020) 2992–3007.
- [14] Y.-C. Chen, M. Meilă, I. G. Kevrekidis, Helmholtzian eigenmap: Topological feature discovery & edge flow learning from point cloud data, *arXiv:2103.07626 [stat.ML]* (2021).
- [15] L.-H. Lim, Hodge Laplacians on graphs, *SIAM Rev.* 62 (3) (2020) 685–715.
- [16] T. M. Roddenberry, M. T. Schaub, M. Hajij, Signal processing on cell complexes, in: *ICASSP 2022-2022 IEEE International Conference on Acoustics, Speech and Signal Processing (ICASSP)*, IEEE, 2022, pp. 8852–8856.
- [17] X. Jiang, L.-H. Lim, Y. Yao, Y. Ye, Statistical ranking and combinatorial Hodge theory, *Math. Program.* 127 (1) (2011) 203–244.
- [18] N. C. Schonsheck, S. C. Schonsheck, Spherical coordinates from persistent cohomology, *J. Appl. Comput. Topol.* (2023) 1–25.
- [19] M. T. Schaub, A. R. Benson, P. Horn, G. Lippner, A. Jadbabaie, Random walks on simplicial complexes and the normalized Hodge 1-Laplacian, *SIAM Rev.* 62 (2) (2020) 353–391.
- [20] S. Ebli, M. Defferrard, G. Spreemann, Simplicial neural networks, *arXiv:2010.03633 [cs.LG]* (2020).
- [21] X. Cheng, X. Chen, S. Mallat, Deep Haar scattering networks, *Information and Inference: A Journal of the IMA* 5 (2) (2016) 105–133.
- [22] T. M. Roddenberry, F. Frantzen, M. T. Schaub, S. Segarra, Hodgelets: Localized spectral representations of flows on simplicial complexes, in: *ICASSP 2022-2022 IEEE International Conference on Acoustics, Speech and Signal Processing (ICASSP)*, IEEE, 2022, pp. 5922–5926.
- [23] D. K. Hammond, P. Vandergheynst, R. Gribonval, Wavelets on graphs via spectral graph theory, *Appl. Comput. Harmon. Anal.* 30 (2) (2011) 129–150.
- [24] C. Battiloro, P. Di Lorenzo, S. Barbarossa, Topological Slepians: Maximally localized representations of signals over simplicial complexes, in: *ICASSP 2023 - 2023 IEEE International Conference on Acoustics, Speech and Signal Processing (ICASSP)*, 2023, pp. 1–5. doi:10.1109/ICASSP49357.2023.10095803.

- [25] J. Chew, M. Hirn, S. Krishnaswamy, D. Needell, M. Perlmutter, H. Steach, S. Viswanath, H.-T. Wu, Geometric scattering on measure spaces, arXiv:2208.08561 [stat.ML] (2022).
- [26] Y. Yang, S. Liu, H. Pan, Y. Liu, X. Tong, PFCNN: Convolutional neural networks on 3D surfaces using parallel frames, in: Proceedings of the IEEE/CVF Conference on Computer Vision and Pattern Recognition, 2020, pp. 13578–13587.
- [27] S. C. Schonsheck, B. Dong, R. Lai, Parallel transport convolution: Deformable convolutional networks on manifold-structured data, *SIAM J. Imaging Sci.* 15 (1) (2022) 367–386.
- [28] J. Irion, N. Saito, Efficient approximation and denoising of graph signals using the multiscale basis dictionaries, *IEEE Transactions on Signal and Information Processing over Networks* 3 (3) (2016) 607–616.
- [29] E. Shvarts, Discrete integral operators on graphs and multiscale transforms on simplicial complexes, PhD dissertation, Appl. Math., Univ. California, Davis (Mar. 2023).
- [30] J. Irion, N. Saito, Hierarchical graph Laplacian eigen transforms, *JSIAM Lett.* 6 (2014) 21–24.
- [31] S. Mallat, *A Wavelet Tour of Signal Processing*, 3rd Edition, Academic Press, Burlington, MA, 2009.
- [32] N. Sharon, Y. Shkolnisky, A class of Laplacian multiwavelets bases for high-dimensional data, *Appl. Comput. Harmon. Anal.* 38 (3) (2015) 420–451.
- [33] W. Lohmiller, J.-J. E. Slotine, On contraction analysis for non-linear systems, *Automatica* 34 (6) (1998) 683–696.
- [34] D. Zou, G. Lerman, Graph convolutional neural networks via scattering, *Appl. Comput. Harmon. Anal.* 49 (3) (2020) 1046–1074.
- [35] C. E. Priebe, D. J. Marchette, Y. Park, E. J. Wegman, J. L. Solka, D. A. Socolinsky, D. Karakos, K. W. Church, R. Guglielmi, R. R. Coifman, D. Lin, D. M. Healy, M. Q. Jacobs, A. Tsao, Iterative denoising for cross-corpus discovery, in: *COMPSTAT 2004—Proceedings in Computational Statistics*, Physica-Verlag HD, 2004, pp. 381–392.
- [36] J. Irion, N. Saito, Learning sparsity and structure of matrices with multiscale graph basis dictionaries, in: A. Uncini, K. Diamantaras, F. A. N. Palmieri, J. Larsen (Eds.), *Proc. 2016 IEEE 26th International Workshop on Machine Learning for Signal Processing (MLSP)*, 2016, pp. 1–6.
- [37] X. Rong, word2vec parameter learning explained, arXiv:1411.2738 [cs.CL] (2016).
- [38] T. M. Tomas, K. Chen, G. Corrado, J. Dean, Q. V. Le, I. Sutskever, word2vec, <https://code.google.com/archive/p/word2vec> (2013).

- [39] F. Pedregosa, G. Varoquaux, A. Gramfort, V. Michel, B. Thirion, O. Grisel, M. Blondel, P. Prettenhofer, R. Weiss, V. Dubourg, J. Vanderplas, A. Passos, D. Cournapeau, M. Brucher, M. Perrot, E. Duchesnay, Scikit-learn: Machine learning in Python, *J. Mach. Learn. Res.* 12 (2011) 2825–2830.
- [40] T. N. Kipf, M. Welling, Semi-supervised classification with graph convolutional networks, *International Conference on Learning Representations* (2017).
URL <https://openreview.net/forum?id=SJU4ayYgl>
- [41] D. Q. Nguyen, T. D. Nguyen, D. Phung, Universal graph transformer self-attention networks, in: *Companion Proceedings of the Web Conference 2022*, 2022, pp. 193–196.
- [42] Y. Wang, Y. Sun, Z. Liu, S. E. Sarma, M. M. Bronstein, J. M. Solomon, Dynamic graph CNN for learning on point clouds, *ACM Trans. Graph.* 38 (5) (2019) Article #146.
- [43] P. Veličković, G. Cucurull, A. Casanova, A. Romero, P. Liò, Y. Bengio, Graph attention networks, *International Conference on Learning Representations* (2018).
URL <https://openreview.net/forum?id=rJXMpikCZ>
- [44] T. Chen, S. Bian, Y. Sun, Are powerful graph neural nets necessary? A dissection on graph classification, *arXiv:1905.04579 [cs.LG]* (2019).
- [45] Meta AI Research, The latest in machine learning papers with code 2023 (2023).
URL <https://paperswithcode.com/>
- [46] J. M. Bowman, C. Qu, R. Conte, A. Nandi, P. L. Houston, Q. Yu, The MD17 datasets from the perspective of datasets for gas-phase “small” molecule potentials, *J. Chem. Phys.* 156 (24) (2022).
- [47] K. Schütt, P.-J. Kindermans, H. E. Sauceda Felix, S. Chmiela, A. Tkatchenko, K.-R. Müller, SchNet: A continuous-filter convolutional neural network for modeling quantum interactions, *Advances in Neural Information Processing Systems* 30 (2017).
- [48] K. T. Schütt, S. S. P. Hessmann, N. W. A. Gebauer, J. Lederer, M. Gastegger, SchNetPack 2.0: A neural network toolbox for atomistic machine learning, *J. Chem. Phys.* 158 (14) (2023).
- [49] K. Schütt, O. Unke, M. Gastegger, Equivariant message passing for the prediction of tensorial properties and molecular spectra, in: *International Conference on Machine Learning*, PMLR, 2021, pp. 9377–9388.
- [50] S. Batzner, A. Musaelian, L. Sun, M. Geiger, J. P. Mailoa, M. Kornbluth, N. Molinari, T. E. Smidt, B. Kozinsky, E (3)-equivariant graph neural networks for data-efficient and accurate interatomic potentials, *Nat. Commun.* 13 (1) (2022) 2453.
- [51] D. S. Weber, On interpreting sonar waveforms via the scattering transform, PhD dissertation, *Appl. Math., Univ. California, Davis* (Dec. 2021).

- [52] P. Yanardag, S. V. N. Vishwanathan, Deep graph kernels, in: Proceedings of the 21th ACM SIGKDD International Conference on Knowledge Discovery and Data Mining, 2015, pp. 1365–1374.
- [53] P. D. Dobson, A. J. Doig, Distinguishing enzyme structures from non-enzymes without alignments, *J. Mol. Biol.* 330 (4) (2003) 771–783.
- [54] A. K. Debnath, R. L. Lopez de Compadre, G. Debnath, A. J. Shusterman, C. Hansch, Structure-activity relationship of mutagenic aromatic and heteroaromatic nitro compounds. correlation with molecular orbital energies and hydrophobicity, *J. Med. Chem.* 34 (2) (1991) 786–797.
- [55] K. M. Borgwardt, C. S. Ong, S. Schönauer, S. V. N. Vishwanathan, A. J. Smola, H.-P. Kriegel, Protein function prediction via graph kernels, *Bioinform.* 21 (suppl_1) (2005) i47–i56.
- [56] H. Toivonen, A. Srinivasan, R. D. King, S. Kramer, C. Helma, Statistical evaluation of the predictive toxicology challenge 2000–2001, *Bioinform.* 19 (10) (2003) 1183–1193.